Pergamon

Int. J. Heat Mass Transfer. Vol. 39, No. 9, pp. 1865–1882, 1996

0017-9310/96 $15.00 + 0.00

0017-9310(95)00290-1

Numerical modelling of variable density turbulent jets

A. GHARBI
Département de Physique, Université de Tunis, Tunisia

E. RUFFIN and F. ANSELMET
IMST, 12, avenue Général Leclerc, 13003 Marseille, France

and

R. SCHIESTEL
IMFM, 1, rue Honnorat, 13003 Marseille, France

(*Received* 20 *February* 1995 *and in final form* 16 *July* 1995)

Abstract—A model of turbulence with second-order closure is used to study the properties of turbulent jets with major variations in density. Validation of the performances of this model, which employs a Favre average procedure, is firstly presented by comparisons with experimental data from scientific literature and those obtained in the specific installation studied at IMST. Special attention is paid to the study of the interface region between the flow and the ambient environment, which demonstrates the present capacities and limitations of this type of model, particularly those associated with the properties related to anisotropy of Reynolds stresses.

1. INTRODUCTION

Low velocity turbulent flows in which the density varies are extremely common in the industrial field and for environmental problems. The density variation can be due to either thermal gradients or the mixture of fluids of different densities, and attention is always paid to the jet momentum dominated region. The properties of such flows are still not fully known and understood, and very few detailed studies have been performed on these flows.

In addition, the numerical prediction of variable density turbulent flows still poses some modelling problems, even if the formalism of the equations has been established for several years [1]. These models can only be developed and perfected by the comparison of experimental data and numerical results [2–11]. Generally speaking, specific studies devoted to variable density flows are rather scarce. It is usually found that only small changes with respect to the standard models developed for constant density flows are required for predicting, with good accuracy, the far-field properties of these jets [12–14] when Favre averaged equations are used. However, new formalisms have recently been proposed which seem to provide better agreement in the intermediate region [15], where the large density gradients especially influence the flow development.

In this article, we propose to use well-established experimental data available in scientific literature to test the performance of second-order closure models. As a basis for comparison, we use (a) the experiments performed by Antonia *et al.* [16, 17] concerning coaxial unheated or slightly heated jets and those experiments presented by Gouldin *et al.* [12] that concern coaxial jets of a propane-air mixture, and (b) the experiment developed at IMST (Amielh *et al.* [18] and Djeridane [19]) in jets of helium, air and CO_2 slightly confined with air co-flow, that are used to study the influence of major density variations (where ρ_J/ρ_e is between 0.14 and 1.52) on the turbulent structure.

The comparisons concern mean values and second-order statistics. Special attention is paid to the analysis of the interface region between the flow and the ambient environment, a problem that had never been addressed before. This clearly demonstrates the present capacities and limitations of this type of model, particularly concerning the properties related to anisotropy of Reynolds stresses. The only criterion available to characterize this region is Phillips' theory, which is used as a reference base. Therefore, in the second part of this work, we present the model used, and the numerical approach for resolution of the equations is described in the third part. The experimental references that provide bases for comparison with the model's predictions are described in the fourth section, and the results obtained are presented and discussed in the fifth section.

NOMENCLATURE

D_J diameter of ejection nozzle
F flatness factor
Fr_J Froude number
$F_{\gamma i}$ turbulent flux components of the scalar, $\widetilde{\gamma u_i}$
$\Im$ intermittence factor
K kinetic energy of turbulence, $1/2R_{ii}$
L_u half-width of mean velocity profile
n_k unit vector normal to wall
r radial coordinate
Re_J Reynolds number at ejection
R_{ij} components of Reynolds stress tensor, $\widetilde{u_i u_j}$
u_i (u, v, w) components of fluctuating velocity (longitudinal, radial and azimuthal)
u', v', w' standard deviations of fluctuating velocity (longitudinal, radial and azimuthal)
U_i $(U, V, 0)$ components of mean velocity (longitudinal, radial)
U_e velocity of co-flow
U_J velocity at ejection
X longitudinal coordinate.

Greek symbols
ε dissipation rate of kinetic energy of turbulence
ε_γ dissipation rate of variance of scalar
χ_n distance from the wall
γ fluctuation of the scalar
γ' standard deviation of scalar fluctuations
Γ instantaneous value of scalar
ρ_J density of the primary jet
ρ_e density of the secondary co-flow.

Conventions
$(\widetilde{\ldots})$ Favre average
$(\ldots)_c$ axial value.

2. TURBULENCE TRANSPORT MODELS

Statistical treatment of the equations of motion and of the scalar (passive or active) is based on average values weighted by mass [1]. These average values have the advantage of providing equations in a form similar to that known in an incompressible situation, complemented by extra terms that introduce density fluctuations. Thus, the modelling formalism [2] can take inspiration from more conventional methods in incompressible flow [3–6].

The models employed are second-order models, which therefore use the Favre average in order to calculate two-dimensional or axisymmetric turbulent flows, which are assumed to be stationary in the mean, with strong density gradients in free or confined configurations. These models also include equations for calculating the properties of the mixture of two gases according to the concentration of one of them (Table 1). Apart from that, our objective is to implement standard second-order models and to investigate their present capacities and limitations for a situation where the experimental conditions are sufficiently well documented.

Table 1. Variable physical properties

Case of temperature: $\Gamma = T$

$$\rho = \rho_0 \frac{T_0}{T} \quad \text{and} \quad \beta = -\frac{1}{\rho}\frac{\partial \rho}{\partial T} = \frac{1}{T}$$

Case of binary mixture (concentration of a constituent): $\Gamma = C$

$$\rho = \frac{\rho_1 \rho_2}{(\rho_2 - \rho_1)C + \rho_1} \quad \text{and}$$

$$\beta = -\frac{1}{\rho}\frac{\partial \rho}{\partial C} = \frac{\rho_2 - \rho_1}{(\rho_2 - \rho_1)C + \rho_1}$$

2.1. *Dynamic model*

Apart from the equations of mean velocity fields ($\tilde{U}$ and $\tilde{V}$), the transport equations to be resolved include those of all Reynolds stress components and that of the dissipation of turbulent kinetic energy. Modelling of the equations of Reynolds stresses (Table 2) is based on the classical models of Hanjalic and Launder [7] and of Launder *et al.* [3]. Among other things, it employs Rotta's hypothesis [8, 9] for non-linear terms of pressure–velocity correlations, and the linear terms are approximated on the basis of the assumption of isotropization of production [3]. As regards the triple correlations of velocity, we use a simplified approximation involving the gradient formulation with anisotropic diffusivity. The contribution of the effects of pressure near the walls is represented by a reflection factor (Φ_{ijw}). The V_{ij} term, representing the correlation between fluctuating velocity and mean pressure gradient, is specific to variable density turbulent flows. It is calculated from the expression for the mean fluctuating velocity $\overline{u_i''} = -(1/\rho)(\partial\bar{\rho}/\partial\Gamma)\,\widetilde{u_i''\gamma''} = \beta F_{\gamma i}$ (where u_i'' represents the fluctuation in Favre's sense, and where $\overline{\rho u_i''} = 0$). We also assumed that the Reynolds stresses dissipation tensor is isotropic (assumption of local isotropy of microturbulence).

The equation for turbulent kinetic energy dissipation (Table 2) is the equation that is normally used. It also refers to the modelling proposed [3, 7]

Table 2. Calculation of Reynolds stresses and dissipation

$$\bar{\rho}\frac{\mathrm{d}R_{ij}}{\mathrm{d}t} = d_{ij} + P_{ij} + V_{ij} + \Phi_{ij} - \varepsilon_{ij} \quad \text{with} \quad \left(\frac{\mathrm{d}}{\mathrm{d}t} \equiv \frac{\partial}{\partial t} + \tilde{U}_k \frac{\partial}{\partial x_k}\right)$$

$$\bar{\rho}\frac{\mathrm{d}\varepsilon}{\mathrm{d}t} = C_\varepsilon\left(\bar{\rho}\frac{K}{\varepsilon}R_{ij}\varepsilon_{,i}\right)_{,j} + \frac{1}{2}C_{\varepsilon 1}P_{kk}\frac{\varepsilon}{K} - C_{\varepsilon 2}\frac{\varepsilon^2}{K} + C_{\varepsilon 4}\frac{\varepsilon}{K}\beta F_{\gamma i}\bar{p}_{,i}$$

$$R_{ij} = \widetilde{u_i u_j} \quad d_{ij} = C_s\left(\bar{\rho}\frac{K}{\varepsilon}R_{ml}R_{ij,l}\right)_{,m}$$

$$P_{ij} = -\bar{\rho}(R_{im}\tilde{U}_{j,m} + R_{jm}\tilde{U}_{i,m})$$

$$V_{ij} = \beta(F_{\gamma j}\bar{p}_i + F_{\gamma i}\bar{p}_{,j}) \quad \text{and} \quad \beta = \frac{1}{\bar{\rho}}\left(\frac{\partial\bar{\rho}}{\partial\tilde{\Gamma}}\right)$$

$$\Phi_{ij} = \Phi_{ij1} + \Phi_{ij2} + \Phi_{ijw} \quad \text{with} \quad \Phi_{ij1} = -C_1\bar{\rho}(\varepsilon/K)(R_{ij} - 2/3K\delta_{ij}) \quad \text{and} \quad \Phi_{ij2} = -C_2(P_{ij} - 1/3P_{kk}\delta_{ij})$$

$$\varepsilon_{ij} = 2/3\bar{\rho}\varepsilon\,\delta_{ij}$$

Wall flow only

$$\Phi_{ijw} = \left[C_1'\bar{\rho}\frac{\varepsilon}{K}\left(R_{km}n_k n_m\delta_{ij} - \frac{3}{2}R_{ik}n_k n_j - \frac{3}{2}R_{jk}n_k n_i\right) + C_2'\left(\Phi_{km2}n_k n_m\delta_{ij} - \frac{3}{2}\Phi_{ik2}n_k n_j - \frac{3}{2}\Phi_{jk2}n_k n_i\right)\right]\frac{K^{3/2}}{C_1\varepsilon\chi_n}$$

Constants

C_1	C_2	C_s	C_ε	$C_{\varepsilon 1}$	$C_{\varepsilon 2}$	$C_{\varepsilon 4}$	C_1'	C_2'	C_1
1.8	0.60	0.22	0.16	1.45	1.90	1.0	0.5	0.3	2.5

and an additional mean pressure gradient term is introduced when the density varies, in a similar manner to the extra production term in the equation for turbulent kinetic energy.

2.2. *Scalar transport model*

The transport equations include the equations for the mean field of the scalar $\tilde{\Gamma}$ responsible for the density variation which can be either the temperature or the concentration of a fluid of different nature to that of the ambient fluid. In addition to these equations, we solve the equations for turbulent scalar fluxes and for the variance of the scalar and of its dissipation, which is calculated by either an algebraic relation or by a transport equation.

Apart from the turbulent fluxes and the dissipation, whose determination is described below, the equation for scalar variance (Table 3) only contains one modelling hypothesis—that of the turbulent diffusion term, which is inspired from the modelling of the diffusion term in the turbulent kinetic energy equation.

Modelling of the scalar dissipation transport equation (Table 3, model 2) is analogous to that of ε. However, it introduces the two characteristic time scales, K/ε and $\gamma^2/2\varepsilon_\gamma$. There is no well-established consensus for this equation in the literature. The constants were chosen and optimized in the heated free jet and the mixing jet presented hereafter. However, Model 1 uses a simpler algebraic relation for calculating scalar dissipation.

The turbulent scalar flux equation (Table 4) is modelled by taking into account similar assumptions

Table 3. Calculation of variance and dissipation of scalar

$$\bar{\rho}\frac{\mathrm{d}\widetilde{\gamma^2}}{\mathrm{d}t} = C_{\gamma\gamma}(\bar{\rho}K/\varepsilon R_{ij}\widetilde{\gamma^2}_{,i})_{,j} - 2\bar{\rho}F_{\gamma i}\tilde{\Gamma}_{,i} - 2\bar{\rho}\varepsilon\gamma$$

Model 1

$$\varepsilon_\gamma = \frac{1}{R}\frac{\varepsilon}{K}\frac{\widetilde{\gamma^2}}{2} \quad \text{where} \quad R = 0.5$$

Model 2

$$\bar{\rho}\frac{\mathrm{d}\varepsilon_\gamma}{\mathrm{d}t} = \mathrm{d}_{\varepsilon_\gamma} + P_{\varepsilon_\gamma} + \varepsilon_{\varepsilon_\gamma}$$

$$\mathrm{d}_{\varepsilon_\gamma} = C_{\varepsilon_\gamma}(\bar{\rho}K/\varepsilon R_{ij}\varepsilon_{\gamma,i})_{,j}$$

$$P_{\varepsilon_\gamma} = -C_{\varepsilon_\gamma 1}\bar{\rho}\varepsilon_\gamma/\widetilde{\gamma^2}F_{\gamma i}\tilde{\Gamma}_{,i} - \mathrm{C}_{\varepsilon_\gamma 2}\bar{\rho}\varepsilon_\gamma/\mathrm{K}\mathrm{R}_{ij}\tilde{\mathrm{U}}_{i,j}$$

$$\varepsilon_{\varepsilon_\gamma} = -C_{\varepsilon_{\gamma\gamma}1}\bar{\rho}\varepsilon_\gamma^2/\widetilde{\gamma^2} - C_{\varepsilon_{\gamma\gamma}2}\bar{\rho}\varepsilon\varepsilon_\gamma/K$$

Constants

C_{ε_γ}	$C_{\varepsilon_\gamma 1}$	$C_{\varepsilon_\gamma 2}$	$C_{\varepsilon_{\gamma\gamma}1}$	$C_{\varepsilon_{\gamma\gamma}2}$	$C_{\gamma\gamma}$
0.16	1.0	1.78	2.0	0.9	0.11

to those made for modelling the Reynolds stress equation. The additional terms $V_{\gamma i}$, which are due to the density variation, are modelled according to the same principles as V_{ij}.

Lastly, in our calculation, we ignored all terms due to gravity, and we used standard constants of models in incompressible conditions (constants recommended by Gibson and Launder [10]).

Table 4. Calculation of scalar flux

$$\bar{\rho}\frac{dF_{\gamma i}}{dt} = d_{\gamma i} + P_{\gamma i} + V_{\gamma i} + \Phi_{\gamma i} - \varepsilon_{\gamma i}$$

$$F_{\gamma i} = \widetilde{\gamma u_i}$$

$$d_{\gamma i} = C_\gamma(\bar{\rho}K/\varepsilon R_{mj}F_{\gamma i,j})_{,m}$$

$$P_{\gamma i} = \bar{\rho}F_{\gamma j}\tilde{U}_{i,j} - \bar{\rho}R_{ij}\tilde{\Gamma}_{,j} \quad \text{and} \quad V_{\gamma i} = \widetilde{\beta_\gamma^2}\bar{p}_{,i}$$

$$\Phi_{\gamma i} = \Phi_{\gamma i1} + \Phi_{\gamma i2}$$

$$\Phi_{\gamma i1} = -C_{\gamma 1}\bar{\rho}(\varepsilon/K)F_{\gamma i} \quad \Phi_{\gamma i2} = +C_{\gamma 2}\bar{\rho}F_{\gamma j}\tilde{U}_{i,j}$$

$$\varepsilon_{\gamma i} = 0.$$

Constants

$C_{\gamma 1}$	$C_{\gamma 2}$	C_γ
3.0	0.33	0.15

3. NUMERICAL APPROACH

3.1. *Discretization of equations*

The above equations (Tables 2, 3 and 4) are all convection–diffusion equations with source terms of the following general form:

$$\frac{\partial\Phi}{\partial t} + \operatorname{div}(\bar{U}\Phi) = \operatorname{div}(\alpha_\Phi \overline{\operatorname{grad}\Phi}) + S_\Phi \qquad (1)$$

which, when applied to the specific case of plane or axisymmetric coordinates, can be written as follows for a flow that is assumed to be stationary:

$$\frac{\partial}{\partial X}(\rho r^j U\Phi) + \frac{\partial}{\partial r}(\rho r^j V\Phi) = \frac{\partial}{\partial X}\left(r^j\alpha_\Phi\frac{\partial\Phi}{\partial X}\right) + \frac{\partial}{\partial r}\left(r^j\alpha_\Phi\frac{\partial\Phi}{\partial r}\right) + r^j S_\Phi. \qquad (2)$$

Therefore, we can consider plane and axisymmetric geometries by taking $j = 0$ and 1, respectively.

The numerical method is based on a finite volumes technique and uses staggered grids for mean velocity components and for turbulent shear stresses and scalar fluxes (Figs. 1 and 2). Huang and Leschziner's stabilization techniques [11] are used to ensure the stability of second-order moments equations and of scalar turbulent fluxes. Note that numerical diffusion induced by the discretization of the convection–diffusion terms has been checked to be reasonably small with the mesh refinement we have used [20].

3.2. *Calculation domain, boundary conditions and meshes*

3.2.1. *Calculation domain.* The calculation domains chosen in the case of free jets and semi-confined jets are shown in Figs. 1 and 2. Different calculation domains can be distinguished: the main domain for calculating the development of the jet and the pre-calculation domains, which provide the main calculation with the conditions at the entry of tube and annular flows, precalculated with the same turbulence models.

3.2.2. *Boundary conditions.* The calculation codes are used to take into account any possible presence of a wall, so that 'confined jet' or 'free jet' calculations can be performed.

Entry conditions

The entry conditions are imposed at the upstream boundary of the flow. At this boundary, we impose Dirichlet conditions that fix the values that the different functions must take. Conditions of this type generally involve experiments that give the most realistic entry conditions. However, since the values of all the functions are not always available, we complete the experimental data with approximations (in particular, for the dissipation rate ε). Another method, used in the case of the experiment performed at IMST, consists in performing a precalculation for a tube and annular space upstream. However, the form of the entry profiles has very little influence on the results outside of the initial region.

Exit conditions

Null gradients are imposed at the exit for all functions V, R_{ij}, $F_{\gamma i}$, ε, ε_γ. Since this assumption is not always realistic, it is preferable to have a calculation domain that is large enough to allow us to suppose that the exit condition does not affect too large a section of the studied domain. The pressure is fixed at the ambient pressure and the component U is deduced from the conservation of mass. In the calculations that we performed, we were able to confirm that the results were only affected in the last two grid lines and far from the most interesting regions.

Wall conditions

A wall is taken into account by using wall functions that impose a value for each function in the first grid division, at a distance from the wall located in the logarithmic region of the velocity profile. The use of these functions avoids having to calculate the development of the fluid layer between the wall and the first calculation grid division: a connection is made with a one-dimensional region adjacent to the wall that is completely integrated.

Free conditions at lateral boundaries

As for the exit conditions, the free boundary conditions at the lateral boundaries are based on the assumption that the gradients of the different values (U, R_{ij}, $F_{\gamma i}$, ε, ε_γ) are equal to zero. If the fluid is going outwards ($V > 0$), we impose a null gradient, but if the fluid is entering ($V < 0$), we impose the fluid properties found outside the domain. The pressure on the free boundary is fixed as equal to the ambient pressure, and velocity V is deduced from the continuity equation.

Symmetry conditions

The centre-line of the jet is an axis of symmetry. Therefore all values at this location have a null partial

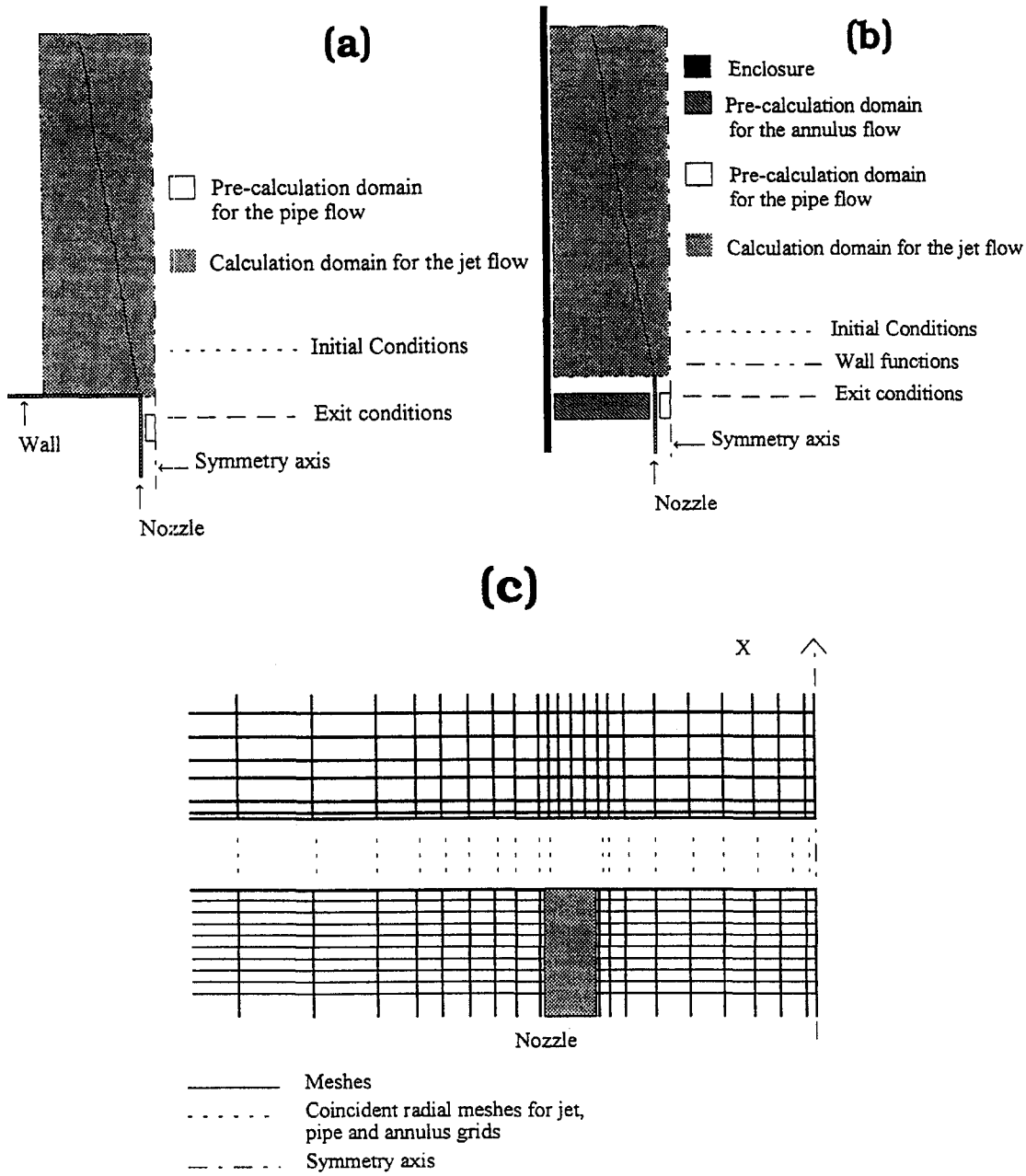

Fig. 1. Calculation domains (a) free jet; (b) confined jet; (c) meshing arrangement.

r derivative, with the exception of $\tilde{V}$, $\tilde{u}\tilde{v}$ and $\tilde{v}\tilde{\gamma}$, which are null on the centreline.

3.2.3. *Meshing.* The study of the solution's sensitivity in relation to the mesh grid is important for determining the useful minimum number of points for a good representation of the different jets. This study was performed in the case of a helium–air jet, since it is in this jet that we find the strongest gradients for all the calculated variables. In particular, we tested the influence of taking or not taking account of a nozzle thickness. All meshes used have two regions where the calculation meshes are more compact: the first is radially around the jet ejection nozzle, and the second is longitudinally in the ejection region ($X/D_J < 20$).

The calculations show that the minimum meshing beyond which the solution becomes insensitive to the number of points is the 64×64 meshing (with 64 axial mesh divisions and 64 radial mesh divisions). Special attention was also paid to the development of jets in the interface region. For this purpose, calculations were performed with finer radial meshes in this region (64×120 points) in order to obtain a very detailed numerical description of the turbulent field for studying the Phillips relations.

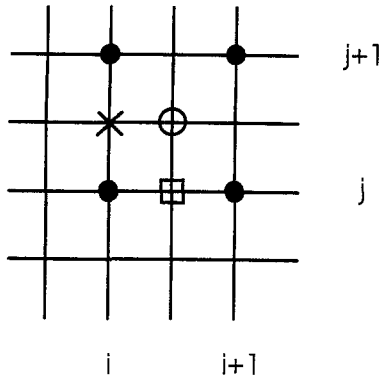

Fig. 2. Localization of the functions on staggered grids. ●: P, K, ε, γ'^2, ε_γ, R_{11}, R_{22}, R_{33}; □: U, $F_{\gamma 1}$; X: V, $F_{\gamma 2}$; ○: R_{12}.

Lastly, it should be noted that most of the calculation code was vectorized (Ruffin *et al.* [20]). Thus the calculation of a jet requires, on average, twenty minutes of CPU time on a Cray YMP-2E computer. The time required is reduced by a factor of around 2.5 with this method of calculation. This factor increases with the number of mesh points.

3.3. *Numerical tests of the imposed conditions*

In the case of the IMST experiment, the values of dissipation rate ε at the entry section were re-adjusted. This is because the tube flow conditions established at the entry are not fully realistic, especially for the helium jet, since the experiment suggests that the development of this jet starts inside the ejection nozzle itself. In addition, the ejection can also create effects due to pressure, since the nozzle has a slightly conical shape in order to reduce its final thickness as much as possible. These two effects can modify the jet's flow in the very first diameters.

Therefore, re-adjustment of the values of ε at the entry in the case of the experimentally studied jets takes these ejection effects into account indirectly, whether they are due to density differences or to pressure effects.

The effects of these corrections are shown in Fig. 3. Note that the adjustment of the dissipation rate in the ejection section of the different jets only influences the initial region within a length of a few diameters ($\approx 5D_j$), but does not have any influence at all on the asymptotic regions of these jets, where the same characteristics are found with or without correction.

4. EXPERIMENTAL REFERENCES

The numerical predictions are compared with four experimental studies that act as tests: a first reference case of constant density flow with isothermal co-flow [16], a slightly heated jet with co-flow [17], measurements by Gouldin *et al.* [12] in a propane jet developing in an annular air jet, and, lastly, the measurements made at IMST [18, 19] in slightly confined jets of helium, air and CO_2 with an air co-flow. All of these experiments are used to compare the results obtained by models presented in different situations covering the different configurations: an isothermal case, a case with very small density variations, and a case with major density variations (ρ_J/ρ_e between 0.14 and 1.55).

4.1. *Free jet of constant density*

The first two references [16, 17] correspond to the case of a constant density jet. The first case is an incompressible unheated jet, and the second is a slightly heated jet therefore temperature can be considered as a passive contaminant.

Antonia and Bilger's measurements [16] show, among other things, the longitudinal variation of the jet's axial velocity and thickness, as well as the level of turbulence. Reynolds stress measurements are also given.

The turbulent jets, developing in an external co-flow of constant velocity, do not have a region of exact similarity. They behave as a pure jet in the initial region if the axial velocity is sufficiently high and their development becomes similar to that of a wake in the more distant region when the axial overspeed is low in relation to the external current's velocity. For a similar configuration to that in ref. [16], the works of Antonia *et al.* [17] provide, among others, the profile of mean temperature, of variance of temperature fluctuations and of turbulent fluxes of heat, which can be useful for comparisons to test the equations of correlations that involve temperature fluctuations.

4.2. *Slightly confined jet of variable density*

The third experiment case [12] concerns a slightly confined jet of propane–air mixture. Although the density difference remains relatively moderate, this case should be considered to involve an active contaminant. The authors provide, among others, the profiles of mean velocity, concentration, Reynolds stresses, and variance of concentration fluctuations. The entry conditions correspond to a virtually laminar jet. In the calculation, however, we introduce a very low level of turbulence in order to allow the use of modelling with a high Reynolds number on entry into the calculation domain.

4.3. *Experiment with jet of high density variation*

The configuration for this experiment [18, 19] is that of an axisymmetric tube jet that is placed vertically and develops in a co-flow. To have more complete control of the boundary conditions for the purposes of numerical calculations, we provided a fully turbulent flow at the ejection. In the light of the works of Pitts [21], we chose to maintain a constant ratio between the jet's momentum and the co-flow's momentum in order to obtain comparable structuration for the different gases. Note that the recent study by Ruffin *et al.* [14] clearly demonstrated that it is indeed this parameter that governs the variation of the different characteristic scales of turbulence in the region of

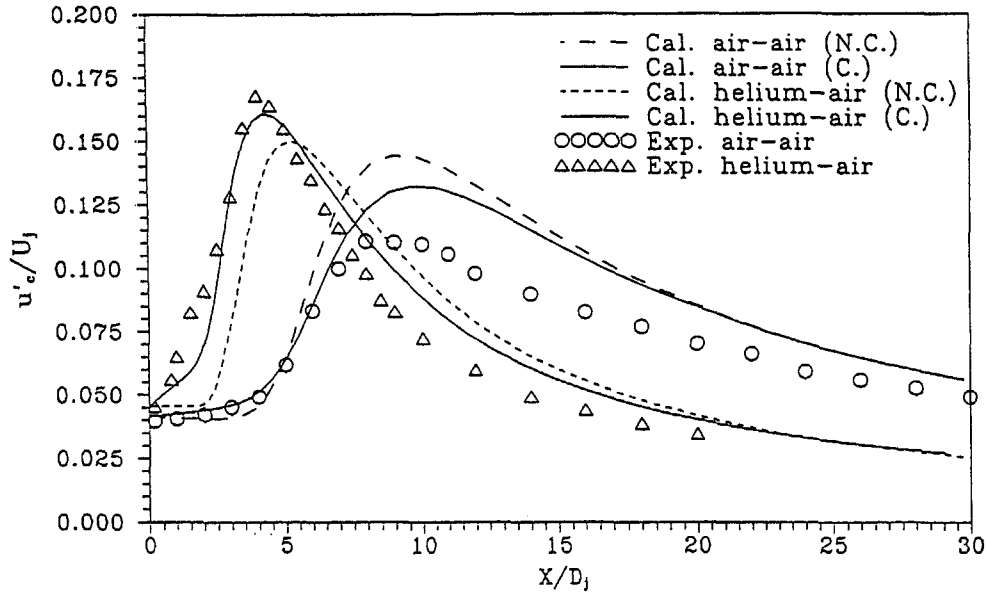

Fig. 3. Axial development of the streamwise velocity standard deviation obtained with different entry conditions for ε.

Table 5

Gas	ρ_J/ρ_e	U_J (m s^{-1})	U_e (m s^{-1})	Re_J	Fr_J
He	0.14	32	1.2	7000	643
Air	1 or 0.94*	12	1.2	21 000	8230
CO_2	1.4	10	1.2	32 000	1363

* Case of passive contaminant ($\Delta T = 20K$).

approximate similarity of variable density jets. Nevertheless, the Reynolds numbers must be sufficiently high to obtain fully turbulent flow at the ejection. Therefore the selected working conditions for the three gases considered are shown in Table 5.

Note that, as explained in refs. [14, 18], we only investigate the flow properties in the region $X/D_J < 40$, where buoyancy effects remain quite small. Indeed, the jet flow for helium is purely momentum dominated up to $X/D_J \approx 20$ and buoyancy becomes dominant only for $X/D_J > 80$. In addition, the co-flow velocity U_e has been chosen to avoid any flow reentry from the downstream exit within the enclosure [18, 19].

5. RESULTS AND DISCUSSIONS

5.1. *Constant density jets and slightly heated jets (approximation of passive contaminant)*

In the case of an isothermal jet [16], the longitudinal variations of axial velocity U_c and of the half-width of the jet are given in Fig. 4. The velocity data is reported in terms of $U_e/\Delta U_c$ in order to highlight the asymptotic hyperbolic decrease of ΔU_c ($= U_c - U_e$). If the qualitative behaviour is correct, the small differences observed would appear to be explained by the well-known inadequacies of standard turbulence models for calculating sheared flows with low production, such as the jet in a co-flow whose behaviour becomes similar to that of a wake in the far-field region.

The results in the case of a slightly heated jet [17] are shown in Figs. 5 and 6. Temperature behaves as a passive contaminant and the variations in density, which are small, have practically no influence on the dynamic field. The good agreement found between the experiment and calculation (except in the external region in which intermittence could perhaps explain the main differences observed) is a preliminary test for the model in a situation with minor density variation. Figure 6 shows the calculation–experiment comparison of temperature variance for two different models of ε_γ: one is based on the assumption that the dynamic and thermal scales are proportional ($R = 0.5$), and the other is based on the equation for the modelled variation of ε_γ (cf. Table 3). In the particular case in question, the latter model gives quite similar results, but the approach is potentially more general.

5.2. *Jets with major density variations*

5.2.1. *Mean field.* The axial variation of mean longitudinal velocity in relation to the position X/D_J is given in Fig. 7. It shows a marked influence of the jets density ratio on their axial decrease, with a more pronounced decrease of $\tilde{U}_c$ when the ratio ρ_J/ρ_e is small. In particular, the helium jet develops more rapidly than the air jet, whose decrease is itself greater than that of the carbon dioxide jet or the propane jet. There is also good correspondence to the measurements obtained by Gouldin *et al.* [12] for the case of a pro-

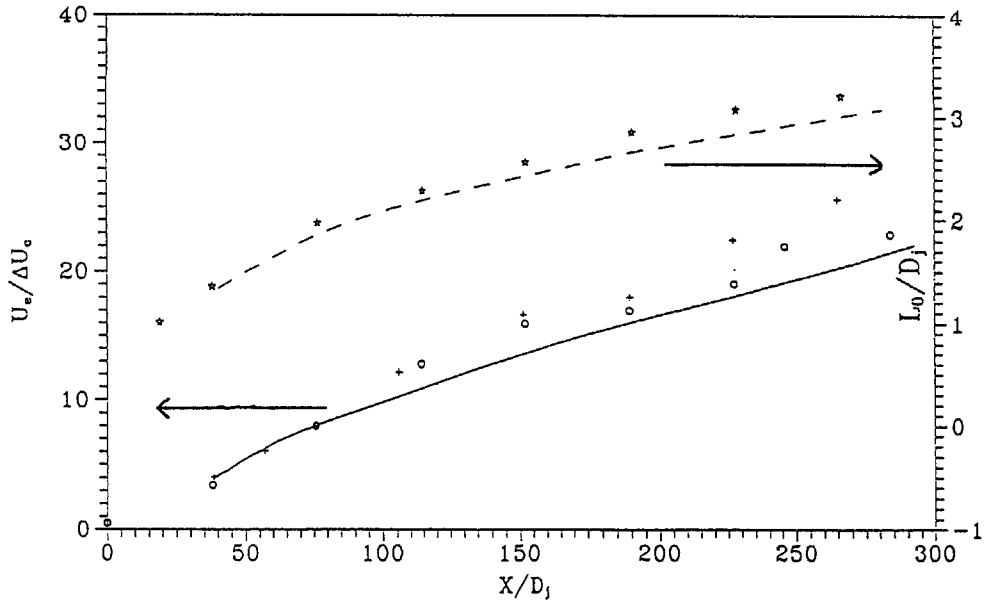

Fig. 4. Axial evolutions of the streamwise velocity (a) and of the associated half-width (b) for the air jet. *: exp. (ref. [12]); ○: exp. (ref. [12], hot wire); +: exp. (ref. [12], Pitot tube); --- and ——: present calculation.

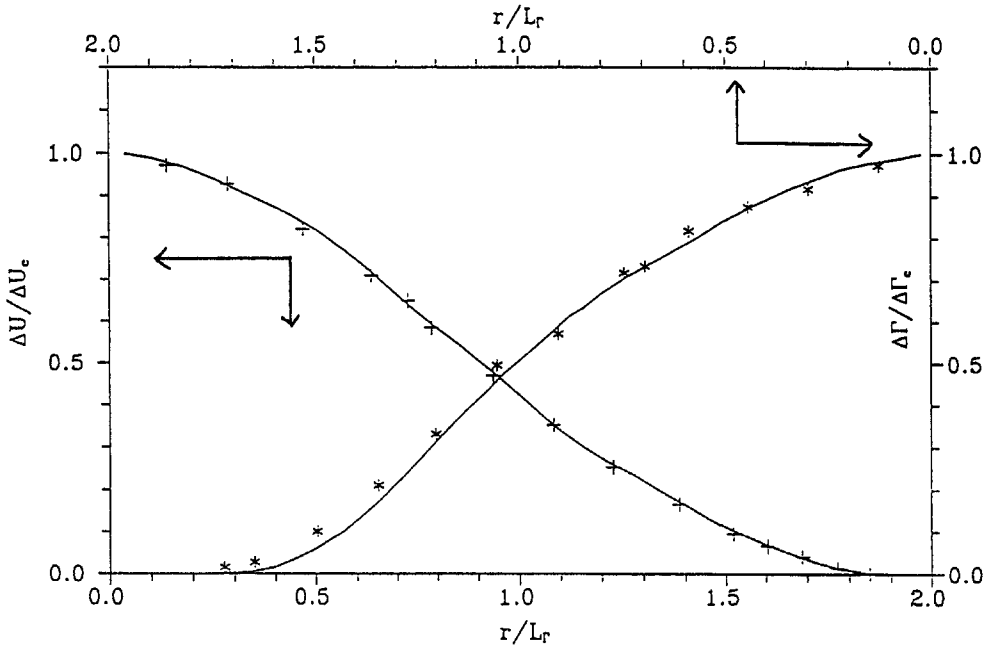

Fig. 5. Radial profiles of the streamwise velocity (a) and of the scalar (b) for the air jet as $X/D_j = 60$. +, *: exp. (ref. [12]); —— present calculation.

pane jet whose density is close to that of carbon dioxide. However, density does not appear to be the only cause of such an effect. Gladnick *et al.* [22] show that the axial decrease in velocity is linked to the initial ratio (U_j/U_e) and to the shape of the initial velocity profile. In the case of the selected working conditions, the ratio U_j/U_e depends directly on the gas in question ($U_j/U_e = 36$, 13, 11 and 5.7, respectively, for helium, air, carbon dioxide and propane). When the latter decreases (at the limit $U_e = 0$ for a free jet), the axial decrease in velocity $\tilde{U}_c$ is accentuated. The numerical profiles are seen to be generally satisfactory. The quality of the numerical predictions for the rate of decrease of longitudinal velocity is acceptable in the case of an air jet, but deteriorates somewhat when the ratio of densities of the two gases moves away from unity. Nevertheless, the rates of decrease obtained by numerical modelling beyond $25D_j(/14/)$ are within the

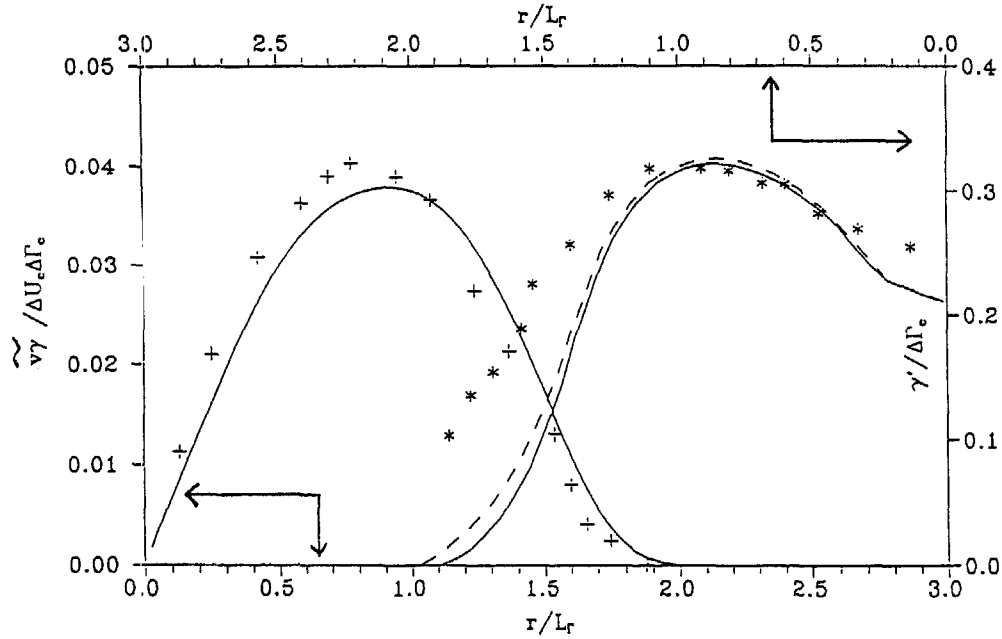

Fig. 6. Radial profiles of the scalar radial turbulent flux (a) and of the scalar standard deviation (b) for the air jet at $X/D_J = 60$. +, *: exp. (ref. [13]); ——: model 1, – – –: model 2, present calculation.

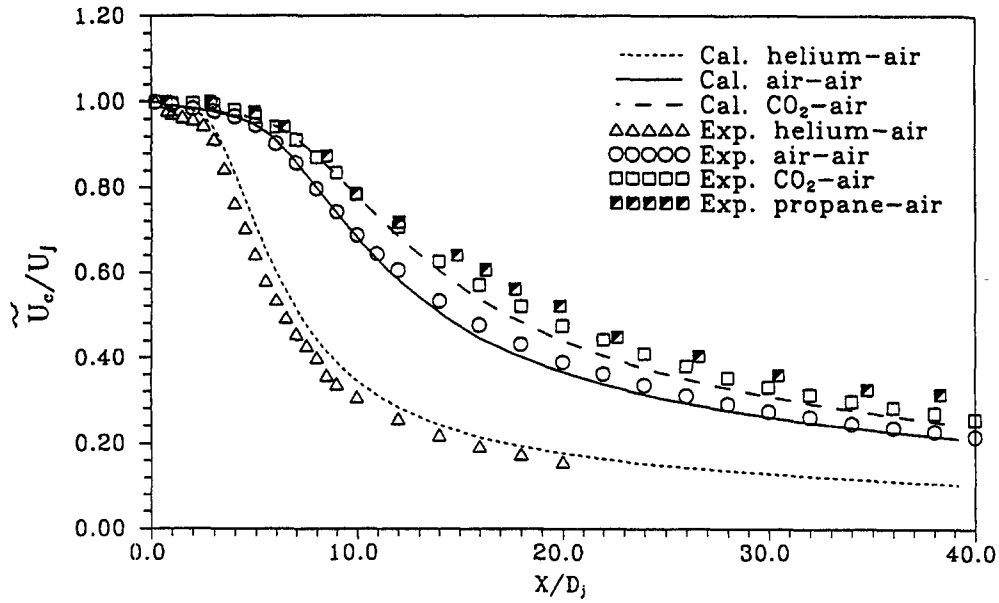

Fig. 7. Axial decrease of the streamwise velocity for the helium, air, carbon dioxide and propane jets.

scatter range of the different experiment data available in literature. It seems that the IMST experiments geometric configuration produces behavioural patterns with slightly higher decrease rates than those normally obtained, which is—mainly for the case of helium—probably due to fact that the jet is slightly confined and also due to the velocity ratio U_J/U_e.

The axial decrease of the scalar field for the different jets is shown in Fig. 8 by the ratio $\tilde{\Gamma}_c/\Gamma_J$. We observe behaviour similar to that of longitudinal velocity $\tilde{U}_c$. The influence of the density ratio is also very marked and, the lighter the gas, the quicker the mass fraction decreases, thereby reflecting a more effective mixture. Here again, the measurements of Gouldin *et al.* [12] are close to those obtained for carbon dioxide. We note that, here again, the calculation–experiment

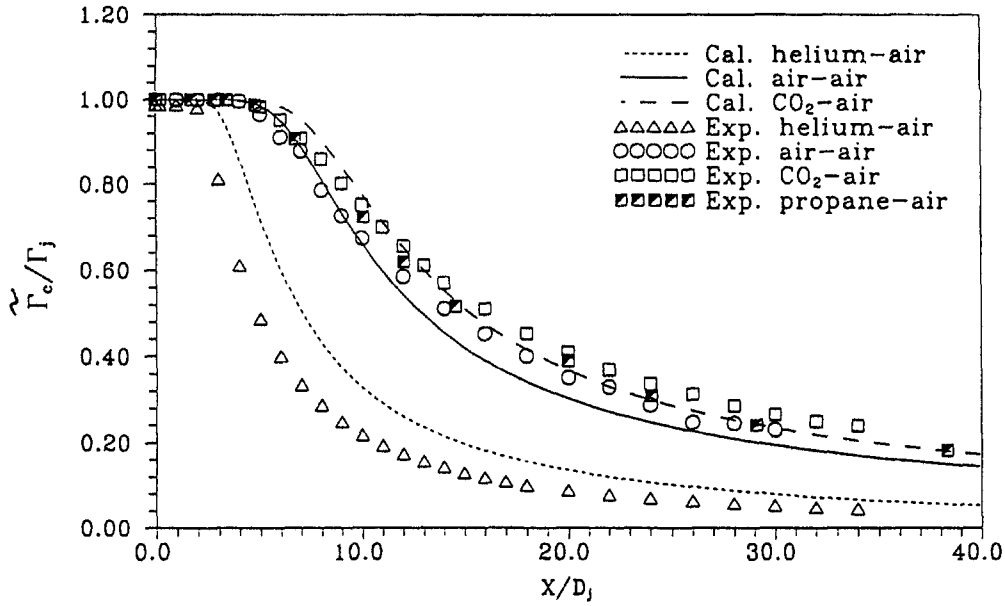

Fig. 8. Axial decrease of the scalar for the helium, air, carbon dioxide and propane jets.

agreement is not so good in the case of helium, for which the density ratio is notably different to unity and the phenomena linked to geometry are more pronounced. Three regions can be distinguished in the representative curves: a first entry region, a second region where it is possible to apply the laws of approximate similarity so that $L_u = A(X-X_0)$, and, lastly, an extreme region where the effects caused by the wall are involved (see ref. [18]). In addition, the spreading rates of the three jets are very similar, except in the near exit region ($X/D_j < 10$) where, in agreement with the experiment, we observe spreading of the CO_2 jet on ejection and, on the other hand, striction of the helium jet (Fig. 9). After this initial region, a difference is observed between the experiment and the calculation: the experiment indicates different spreading for the three jets, while the calculations give very similar results. This effect is still quite difficult to explain. Some studies attribute this phenomenon to the Reynolds number and others to the jet/co-flow velocity ratio or to the ejection conditions (laminar or fully turbulent), which also amounts to a Reynolds number

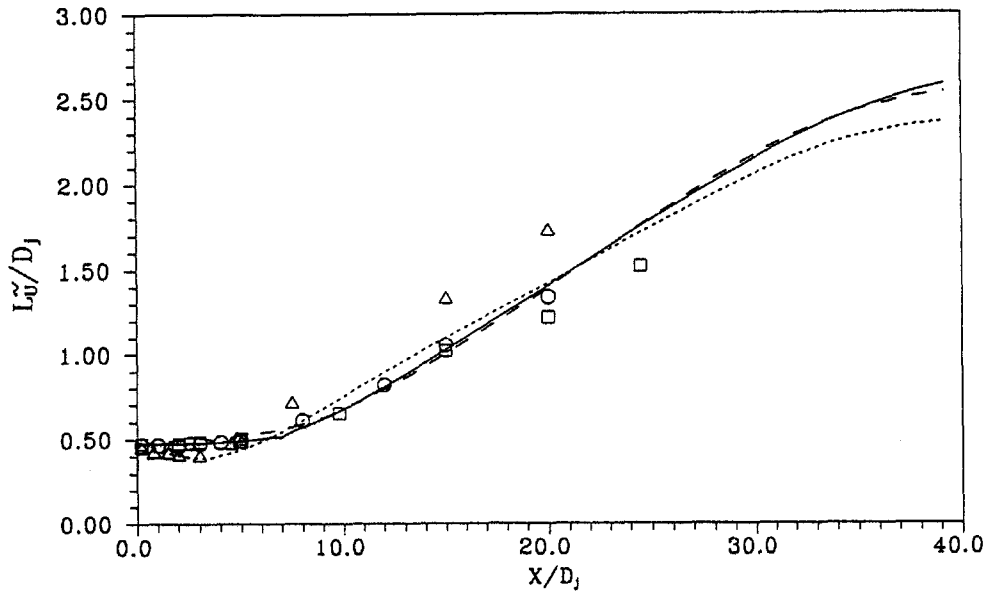

Fig. 9. Streamwise velocity half-widths for the helium, air and carbon dioxide jets. Helium: △ (exp.) and --- (calculation); air: ○ and ——; carbon dioxide: □ and ---.

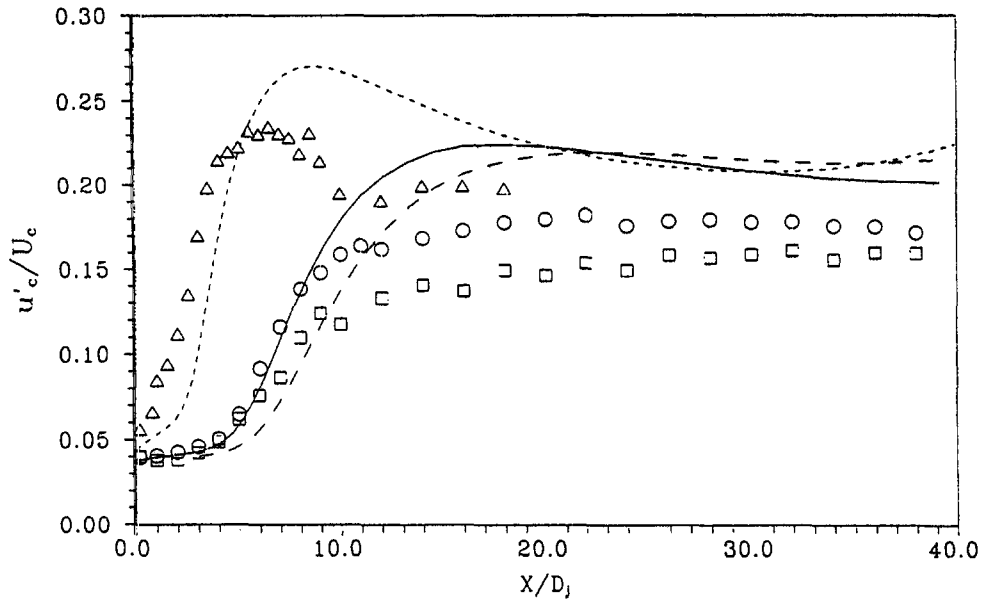

Fig. 10. Axial evolution of the streamwise velocity turbulence intensity. Same symbols as for Fig. 9.

effect (see refs. [18, 23]). Note that the radial global properties for the scalar field are not reported herein since they are rather similar to those for the dynamic field as discussed in detail in Ruffin *et al.* [14].

Therefore, it seems that taking into account the additional factors that appear in the case where the density varies is not enough to correctly determine the subtle influence of this variation on the dynamic field.

5.2.2. *Turbulent field.* As regards the axial variations of turbulent values, particularly the standard deviations of longitudinal velocity fluctuations and of the passive contaminant, rendered dimensionless, respectively, by the values on the axis, $\tilde{U}_c$ and $\tilde{\Gamma}_c$, of $\tilde{U}$ and $\tilde{\Gamma}$ in the different gas jets, the results are given in Figs. 10 and 11. We observe that, in the case of the lighter-than-air jet, the initial increase of the turbulent intensity occurs much sooner. And thus, regarding the turbulent dynamic field, the asymptotic trend is reached more rapidly when ρ_j/ρ_e is low. However, the asymptotic value seems to be common to the three gases. Note that, for the velocity field, we reported the quantities $u'_c/\tilde{U}_c$ and not $u'_c/(\tilde{U}_c - U_e)$, whose asymp-

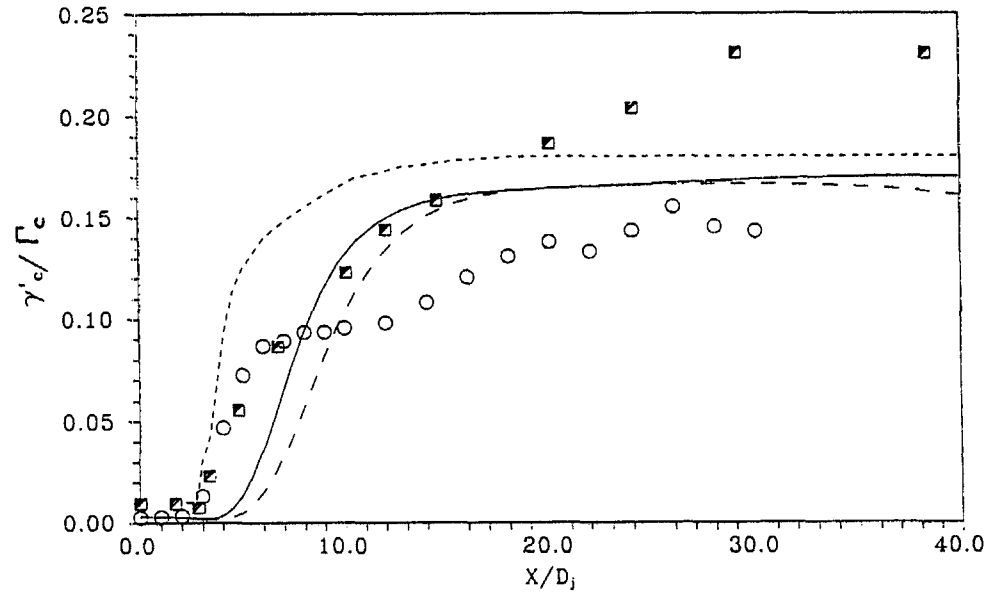

Fig. 11. Axial evolution of the scalar turbulence intensity for the helium, air and propane jets. Helium: --- (calculation); air: ○ (exp.) and —— (calculation); propane: ◩ and - - -

totic level is not directly comparable to the usual results obtained in free jets. The values of $u'_c/(\bar{U}_c - U_e)$, which are close to 0.25, are in very good agreement (ref. [14]) with classical values. The results obtained for the turbulent scalar field are not as good as those for the dynamic field. In this case, the calculations also show a noteworthy trend towards an asymptotic value when using normalization by the axial mean scalar values. This is in good agreement with Pitts' experiments [20]. In the case of the air jet, the axial variation of the standard deviation of the passive contaminant γ is shifted in relation to the experimental profile, but the general form is quite clearly determined. The only modelling hypotheses involved in the scalar variance equation were those of turbulent diffusion and of dissipation. Therefore it is probable that the differences between the experiment and the calculation for the air jet are caused by the modelling of the equation of dissipation in the initial region covering the very first diameters. These differences can also be partly due to differences already observed in the experimental and numerical dynamic fields because, in case of the passive contaminant, the scalar field does not affect the dynamic field, but is simply transported by it. Besides, the results obtained for temperature variance at a distance of 20 diameters are in good agreement (turbulent rates are slightly less than 0.2) with those of Chua and Antonia [24].

5.3. *Study of the near exit region*

5.3.1. *Study at various cross-sections of the jet.* The radial profiles of the standard deviations of the longitudinal velocity fluctuations normalized by the mean velocity U_J vs r/D_J for different cross-sections are shown for helium and air, respectively, in Figs. 12(a), (b). The general appearance of the results obtained shows that, since the mixture is more rapid in the light jets ($\rho_J/\rho_e < 1$), the radial profiles of standard deviations spread more rapidly and reach an asymptotic shape. The opposite behaviour is obtained in the case of the heavy jets ($\rho_J/\rho_e > 1$), with much slower spreading, but these results are not given here. The model gives good results, mainly for the intensity of peaks of the standard deviations of longitudinal velocity. The shapes of these profiles are also clearly determined, particularly regarding their rapid developments towards pseudo-asymptotic behaviour and their widths, in the first diameters of the helium-air jet. Thus, in the case of the helium–air mixture, when $X/D_J = 2$, the profiles correspond to the merging of the boundary layers surrounding the nozzle, which causes a clearly visible peak of turbulent energy. On the other hand, when $X/D_J = 5$, we already obtain a distribution that is reminiscent of a typical jet profile in a similarity region, while, above $X/D_J = 15$, with the spreading of the energy distribution, the effects of confinement can be detected.

5.3.2. *Phillips' laws at the external boundary.* Phillips' theory [25] establishes two relations that are valid in the intermittence region. These two relations correspond to the following in the case of an axisymmetric jet:

(a) The energy of fluctuations induced at the interface for the three components of velocity decrease in inverse proportion to the fourth power of the distance from the centre of the jet:

$$u'^2, v'^2, w'^2 \propto (y - y_0)^{-4}, \tag{3}$$

where y_0 is the virtual origin of the irrotational flow.

(b) the energy relative to the fluctuation of the radial velocity component is equal to the sum of the energies of the other two components:

$$v'^2 = u'^2 + w'^2. \tag{4}$$

Figures 13(a)–14(b) show the radial profiles of the standard deviations of velocity fluctuations to the power of $-1/2$ (or variances to the power of $-1/4$) in terms of their respective values on the jet axis, i.e. $u_c'^{-1/2}$, $v_c'^{-1/2}$, $w_c'^{-1/2}$, and the variation of the intermittence factor $\mathfrak{I} = 3/F_u$ (where F_u is the flatness factor of u, $F_u = \overline{u^4}/\overline{u^2}^2$) vs the similarity parameter r/L_u (where L_u is the half-width of the longitudinal velocity profiles) for air and for helium. The results group together to a certain extent, thus demonstrating the presence of three main regions of the flow:

(1) A first region around the axis, which extends as far as the start of the interface, where the ratios u'/u'_c, $v'/'_c$ and w'/w'_c practically do not vary at all and display plateaus at a value almost equal to unity. However, for the air flow, in the near-field region ($X/D_J = 5$), the variations are larger as the radial velocity profiles are not yet developed. On the contrary, for the helium flow at the same station, the almost asymptotic shape appears as already attained. The turbulent jet actually develops in this region. In fact, in this non-intermittent region, the values of the flatness factor F_u seem to be nearer 2.8 than 3 (3 corresponds to a perfectly Gaussian distribution). Consequently, the values of the intermittence factor $\mathfrak{I}$ exceed (paradoxically) unity, since $\mathfrak{I}$ was determined by the standard method giving $\mathfrak{I} = 3/F_u$, which is based on the assumption that turbulence is distributed in a Gaussian manner and that there is an all-or-nothing phenomenon (Dumas [26]).

(2) A second region that is of very real interest for us, which is the region separating the fully turbulent flow from the co-flow. This region is not very extensive at the nozzle exit. The measurement points are not sufficiently close together to allow us to draw a clear conclusion regarding the influence of density. However, for distances from the jet centre of between $r/L_u = 2$ and $r/L_u = 3$, where we find intermittence factors of less than 0.5 that decrease as far as around 0.15, it seems that energy of turbulent fluctuations does indeed vary according to $(r/L_u)^{-1/4}$ in a way similar to Phillips' prediction (3). In addition, Figs. 14(a), (b) point to a close similarity of the widths of the intermittent regions (roughly lying between 2.2 and 3 L_u) for air and for helium, at respective cross-

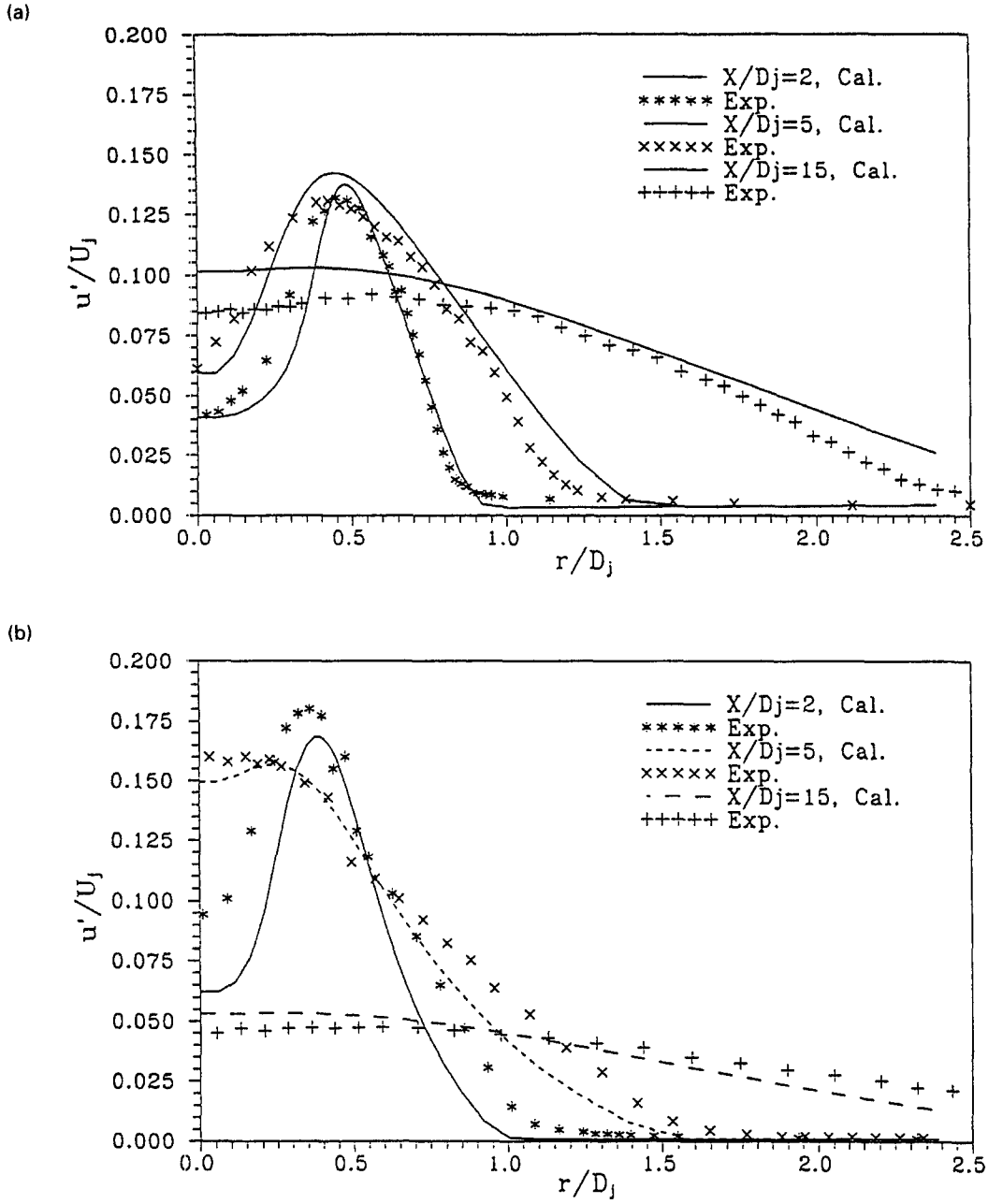

Fig. 12. Radial profiles of the streamwise velocity standard deviation for the air (a) and helium (b) jets.

sections $X/D_J = 20$ and $X/D_J = 15$, although, for the helium jet, the radial profile measurements are not performed far enough from the axis to be able to obtain the variations of the velocity variances beyond $r/L_u = 2.5$.

(3) A third region where turbulent tube co-flow is found, since we are approaching the walls of the experimental confinement working section. As in the case of the first region, the values of the intermittence factor paradoxically exceed unity. On the other hand, the level of turbulence is very low in this region compared to that obtained on the axis, but it is not null (the turbulence intensity is between 5 and 10% depending on the considered gas and on the particular section).

It seems clear that the model implemented provides correct predetermination of the measurements, particularly in the first and second regions described above. However, in the third region, the difference observed between the calculation and the experiments could be linked to the effects of confinement.

In order to test the validity of Phillips' second law,

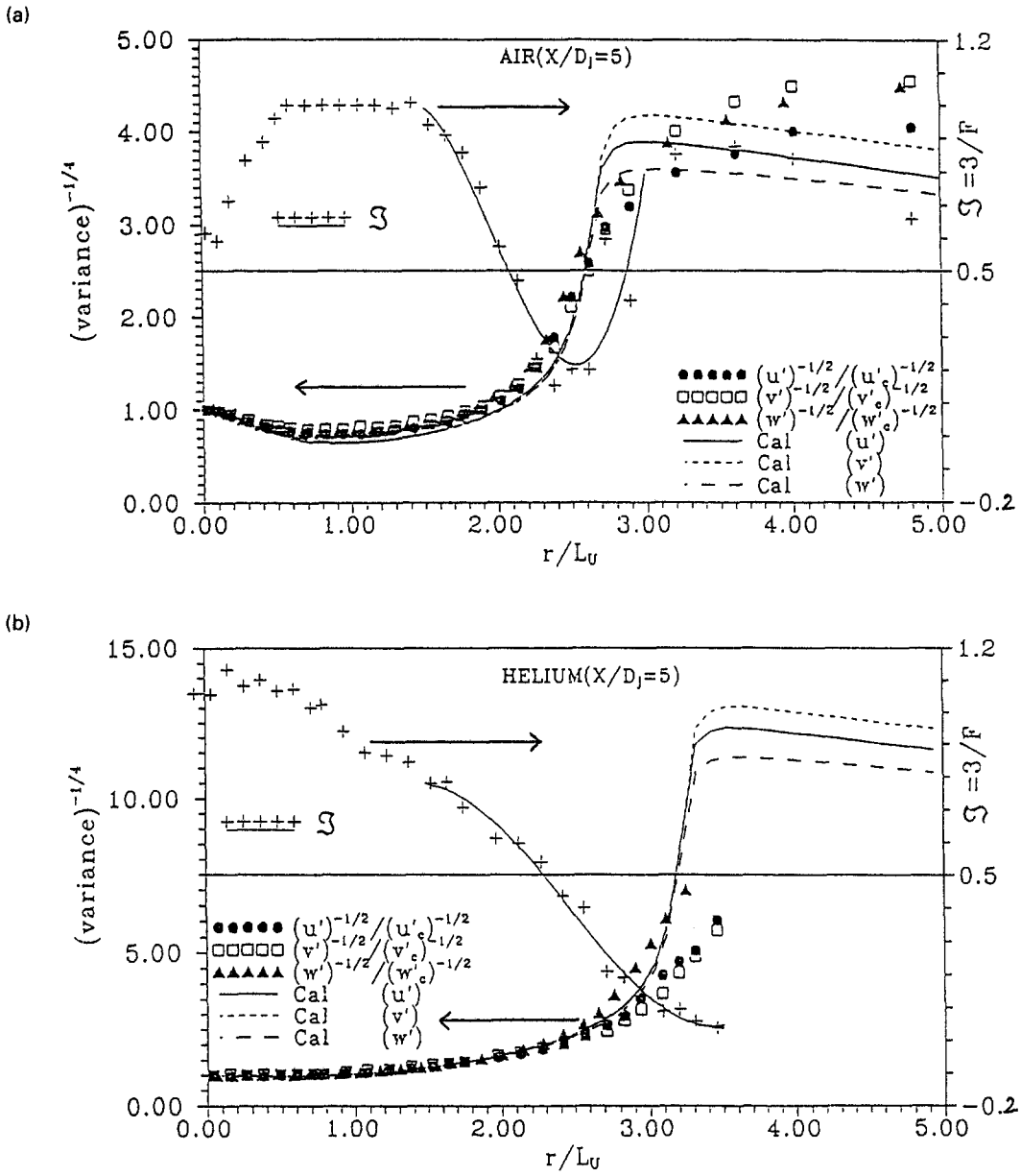

Fig. 13. Validity test for Phillips' first law at $X/D_J = 5$ for the air (a) and helium (b) jets.

we analyzed the energy of fluctuation of the radial component in relation to the sum of the energies of the two other velocity components. The simultaneous representation of the radial variation of the variable $((u'^2+w'^2)/v'^2)-1$ and of the intermittence factor informs us of the domain of validity of this law. In fact, Figs. 15(a)–16(b) show that, for values of $\Im$ lower than 0.5 and tending towards zero, we obtain nullity of the variable $((u'^2+w'^2)/v'^2)-1$ for the two jets, but in less extensive domains than those found in the verification of the first law. These results are compatible with those of Antonia *et al.* [27] and those of Fabris [28] for air flows, which confirm Phillips' second law for the lowest values of the intermittence factor ($\Im < 0.2$). Phillips [25] calculated the velocity field induced by turbulent fluctuations in an incompressible fluid. His assumptions are based on the observations of Townsend [29], assuming that the induced random velocity field is rotational. He then shows that the second law is confirmed in the range $0.04 < \Im < 0.11$. However, the validity of this law is consequence of irrotationality of the flow and of its uniformity. This last condition is only satisfied in the case where $\Im$ has a low value. Wyganski and Fiedler [30] state that the verification of this law for a layer of mixture also depends on the domain of study.

As opposed to the verification of Phillips' first law, the second-order model in the standard version used

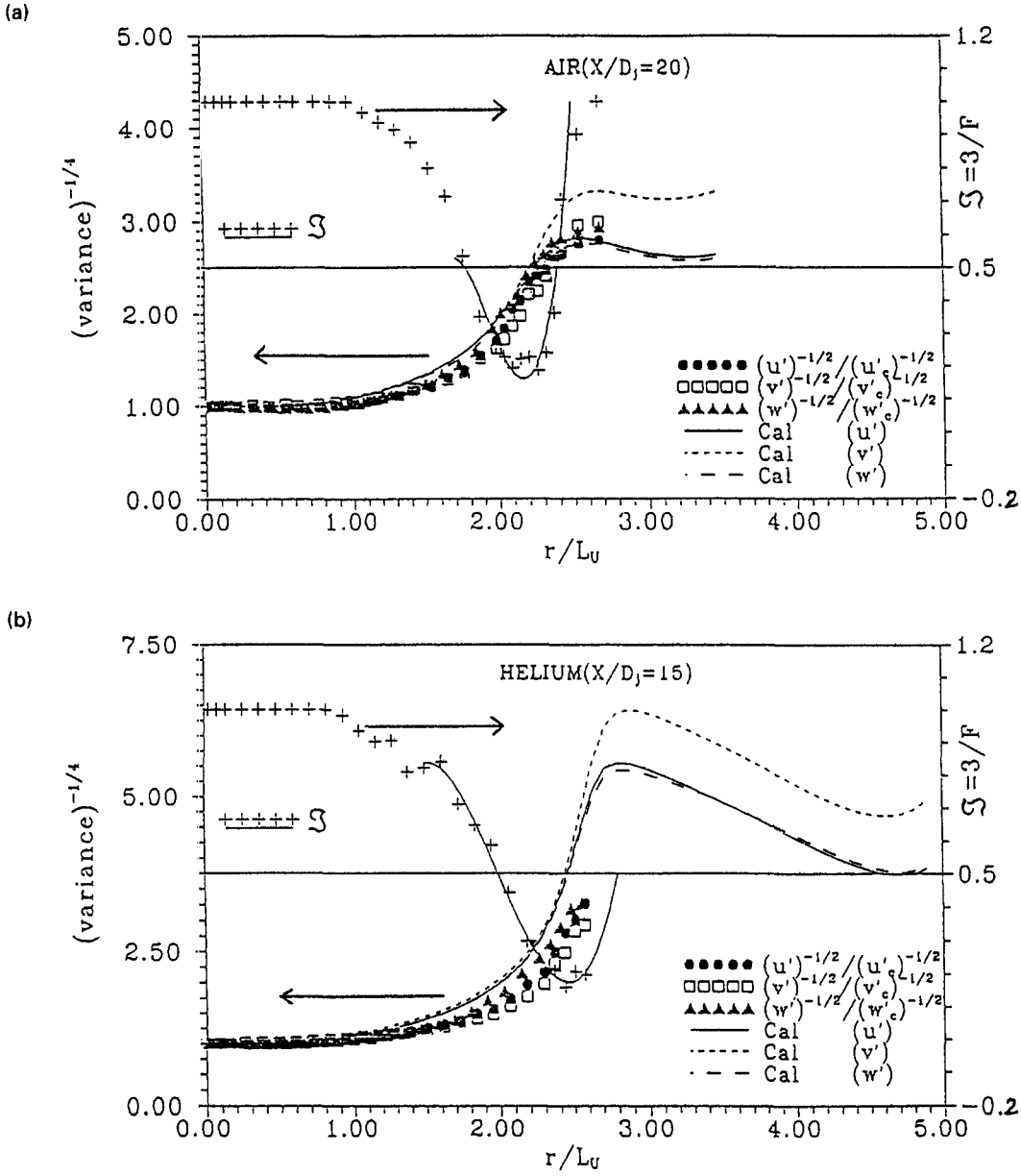

Fig. 14. Validity test for Phillips' first law at $X/D_J = 20$ for the air jet (a) and at $X/D_J = 15$ for the helium jet (b).

here does not appear to be able to provide a suitable description of the measurements. This reflects the fact that this type of model still has inadequacies in the detailed description of anisotropy of the turbulent field [31].

6. CONCLUSION

This study enabled us to specify the performance and inadequacies of a standard second-order model based on Favre averages in the case of variable density jets. This modelling is used to satisfactorily represent both the case of incompressible jets or slightly heated jets and the case of mixtures with low density variations. The results obtained in the far field region are quite good. On the other hand, it is found that improvements are necessary to represent the regions of high density gradient and also, in general, the turbulent field in the initial region.

We also found that, independently of the problems due to density variations, there are some well-known difficulties in correctly representing the development

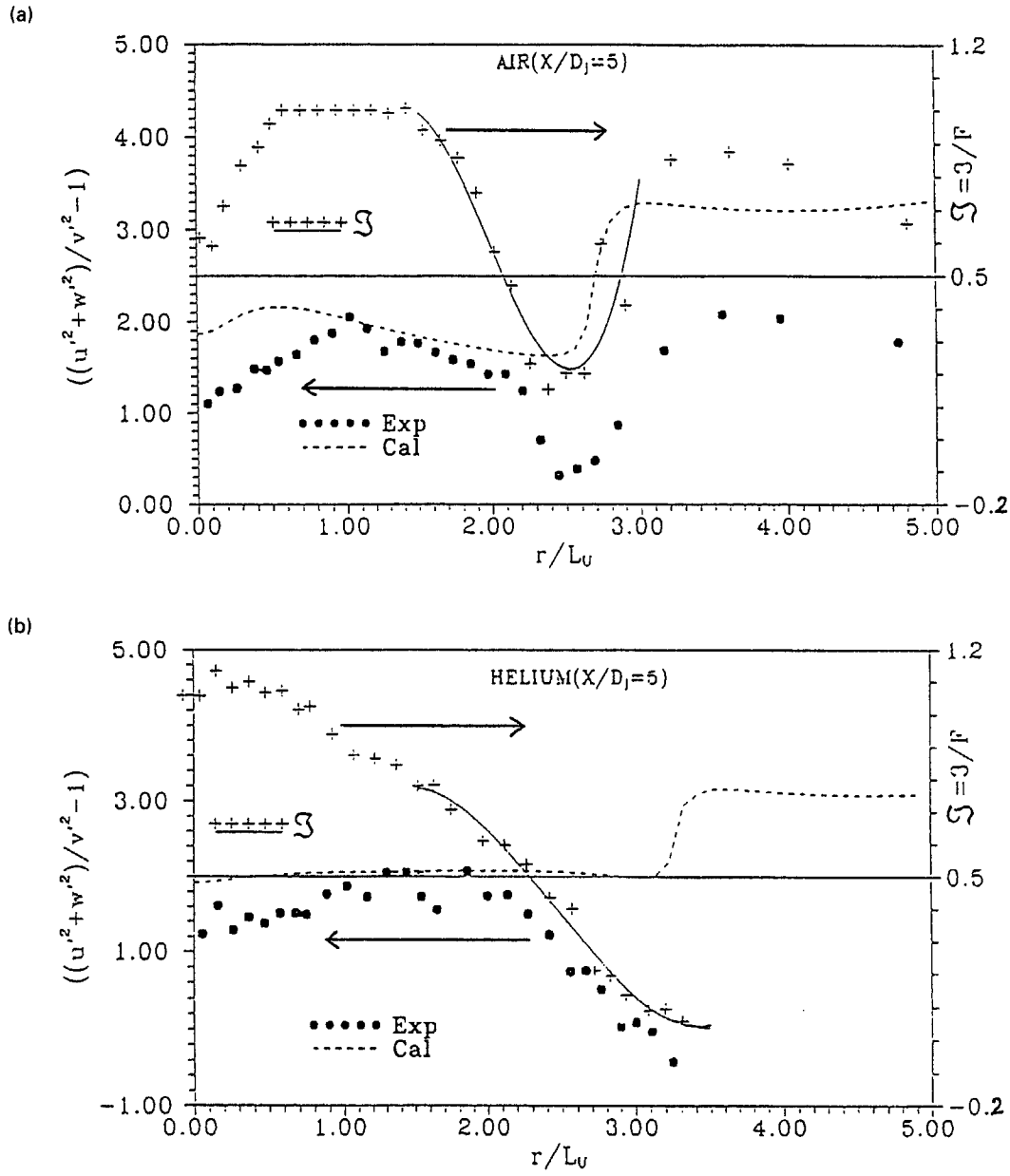

Fig. 15. Validity test for Phillips' second law at $X/D_J = 5$ for the air (a) and helium (b) jets.

of pure air jets. More correct modelling of constant density turbulence will be required, as well as modelling of the effects due to high density gradients. For this purpose, the new generation of models (ref. [32]) should bring useful advances.

However, the version of the model used provides a quite correct representation of the influence of these major density variations on the variations of mean values and on the turbulent field. Although this description may be sufficient for many practical applications, it contains some inadequacies that are particularly evident in the initial region of the jets where the variations of the different values are much more rapid. In addition, the differences found are generally more marked in the scalar field than in the dynamic field.

The study of the interface region revealed a behaviour that is entirely compatible with Phillips' first law that characterizes the radial variations of turbulent stresses in the intermittent region. The results are quite remarkably grouped together for the different gases considered. Phillips' second law—which is linked to

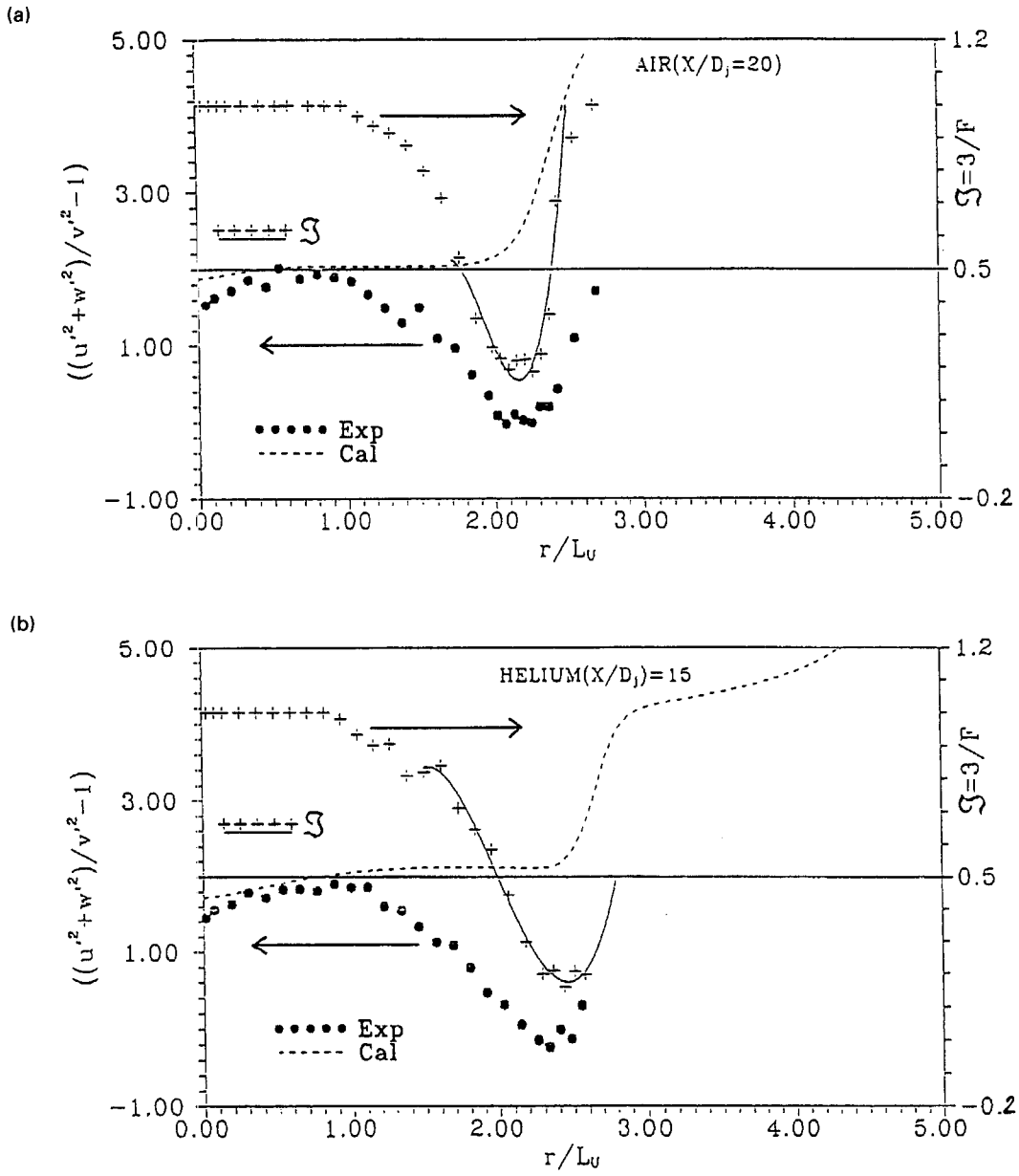

Fig. 16. Validity test for Phillips' second law at $X/D_J = 20$ for the air jet (a) and at $X/D_J = 15$ for the helium jet (b).

the anisotropy of the Reynolds tensor in this region even if its domain of validity seems to be more limited—is much less well represented by the calculation. This is, of course, a very severe test for a model, because the calculated anisotropy is the result of crucial assumptions concerning pressure correlations in particular, which are well known to be complex. One should also note the influence of intermittence, which is not explicitly taken into account in the model.

Acknowledgements—Financial support from EDF, GDF, INERIS, SNECMA and the PACA Regional Council is gratefully acknowledged. L. Fulachier, M. Amielh and T. Djeridane provided considerable help for the development of this research at IMST and for collecting the experimental data analyzed herein. F. Anselmet thanks J. C. R. Hunt for an interesting discussion that significantly influenced this study.

REFERENCES

1. A. Favre, Equations des gaz turbulents compressibles, *J. Mécanique* **4**, 361–390 (1965) and **4**, 390–421 (1965).

2. A. Gharbi, R. Schiestel and F. Anselmet, Modélisation numérique de jets turbulents à densité variable à l'aide de fermetures au second-ordre, Note no. 94/2, Institut de Mécanique de Marseille (1994).
3. B. E. Launder, G. J. Reece and W. Rodi, Progress in the development of a Reynolds turbulence closure, *J. Fluid Mech.* **68,** 537–566 (1975).
4. B. E. Launder, Turbulence models and their applications, In *Second Moment Closure, Methodology and Practice* (Edited by B. E. Launder, W. C. Reynolds, W. Rodi, J. Methven and D. Jeandel), Vol. 2. Eyrolles, Paris (1984).
5. R. Schiestel, *Modélisation et Simulation des écoulements turbulents, Traité des Nouvelles Technologies*, Série Mécanique. Hermes, Paris (1993).
6. D. Vandromme, H. Ha Minh, J. R. Viegas, M. W. Rubesin and W. Kollmann, Second-order closure for the calculation of compressible bounded flows with an implicit Navier–Stokes solver. In *Proceedings of the 4th International Symposium on Turbulent Shear Flows*, Karlsruhe (1983).
7. K. Hanjalic and B. E. Launder, A Reynolds stress model of turbulence and its application to thin shear flows. *J. Fluid Mech.* **52,** 609–638 (1972).
8. J. Rotta, Statitische Theorie nichthomogener Turbulenz Part I, *Z. Phys.* **129,** 547–573 (1951).
9. J. Rotta, Statistiche Theorie nichthomogener Turbulenz Part II, *Z. Phys.* **131,** 51–77 (1951).
10. M. M. Gibson and B. E. Launder, Ground effects on pressure fluctuations in the atmospheric boundary layer, *J. Fluid Mech.* **86,** 491–511 (1978).
11. P. G. Huang and M. A. Leschziner, Stabilisation of recirculating flow computations performed with a second moment closure and third order discretisation. In *Proceedings of the 5th International Symposium on Turbulent Shear Flows*, Cornell University (1985).
12. F. C. Gouldin, R. W. Schefer, S. C. Johnson and W. Kollman, Non reacting turbulent mixing flows, *Prog. Energy Combust. Sci.* **12,** 257–303 (1986).
13. N. R. Panchakapesan and J. L. Lumley, Turbulence measurements in axisymmetric jets of air and helium, Part 2, Helium jet, *J. Fluid Mech.* **246,** 225–247 (1993).
14. E. Ruffin, R. Schiestel, F. Anselmet, M. Amielh and L. Fulachier, Investigation of characteristic scales in variable density turbulent jets using a second-order model, *Phys. Fluids* **6,** 2785–2799 (1994).
15. P. Chassaing, G. Harran and L. Joly, Density fluctuation correlations in free turbulent binary mixing, *J. Fluid Mech.* **279,** 239–252 (1994).
16. R. A. Antonia and R. W. Bilger, An experimental investigation of an axisymmetric jet in a co-flowing stream, *J. Fluid Mech.* **61,** 805–822 (1973).
17. R. A. Antonia, A. Prabhu and S. E. Stephenson, Conditionally sampled measurements in a heated turbulent jet, *J. Fluid Mech.* **72,** 455–480 (1975).
18. M. Amielh, T. Djeridane, F. Anselmet and L. Fulachier, Velocity near-field of variable density turbulent flows, *Int. J. Heat Mass Transfer* (in press).
19. T. Djeridane, Contribution à l'étude expérimentale de jets turbulents axisymétriques à densité variable, Ph.D. thesis, University of Aix-Marseille II (1994).
20. E. Ruffin, R. Schiestel, F. Anselmet and L. Fulachier, Modélisation du second-ordre de jets turbulents à masse volumique variable, Note no. 93/5, I.M.S.T., Marseille (1993).
21. W. M. Pitts, Effects of global density and Reynolds number variations on mixing in turbulent axisymmetric jets, Report NBSIR 86-3340, Department of Commerce, Washington (1986).
22. P. G. Gladnick, A. C. Enotiadis, J. C. La Rue and G. S. Samuelsen, Near-field characteristics of a turbulent coflowing jet, *AIAA J.* **28,** 1405–1414 (1986).
23. R. A. Antonia, B. R. Satyaprakash and A. K. M. F. Hussain, Measurements of dissipation rate and some other characteristics of turbulent plane and circular jets, *Phys. Fluids* **23,** 695–700 (1980).
24. L. P. Chua and R. A. Antonia, Turbulent Prandtl number in a circular jet, *Int. J. Heat Mass Transfer* **33,** 331–339 (1990).
25. O. M. Phillips, The irrotational motion outside a free turbulent boundary, *Proc. Cambridge Philos. Soc.* **51,** 220–229 (1955).
26. R. Dumas, Contribution à l'étude des spectres de turbulence, *Publ. Scient. Techn. Min. Air* **404** (1964).
27. R. A. Antonia, D. A. Shah and L. W. B. Browne, The organised motion outside a turbulent wake, *Phys. Fluids* **30,** 2040–2045 (1987).
28. G. Fabris, Conditional sampling study of the turbulent wake of a cylinder Part 1, *J. Fluid Mech.* **94,** 673–710 (1979).
29. A. A. Townsend, *The Structure of Turbulent Shear Flow*. Cambridge University Press, London (1956).
30. I. Wygnanski and H. E. Fiedler, The two-dimensional mixing region, *J. Fluid Mech.* **41,** 327–361 (1970).
31. E. Ruffin, Etude de jets turbulents à densité variable à l'aide de modèles de transport au second ordre, Ph.D. thesis, University of Aix-Marseille II (1994).
32. B. E. Launder, Second-moment closures: present ... and future?, *Int. J. Heat Fluid Flow* **10,** 282–300 (1989).